

See discussions, stats, and author profiles for this publication at: <https://www.researchgate.net/publication/230888226>


# The role of mangroves in attenuating storm surges

**Article** in *Estuarine Coastal and Shelf Science* · May 2012  
DOI: 10.1016/j.ecss.2012.02.021

CITATIONS  
120


READS  
560

7 authors, including:




**Keqi Zhang**  
Florida International University  
**63** PUBLICATIONS **2,823** CITATIONS

SEE PROFILE




**Huiqing Liu**  
North Carolina State University  
**18** PUBLICATIONS **342** CITATIONS

SEE PROFILE



**Yuepeng Li**  
Florida International University  
**17** PUBLICATIONS **218** CITATIONS


SEE PROFILE




**Hongzhou Xu**  
Institute of Deep-sea Science and Engineering, Chinese Academy ...  
**17** PUBLICATIONS **442** CITATIONS

SEE PROFILE

Some of the authors of this publication are also working on these related projects:

- 

Create new project "Applications of LIDAR data" [View project](#)
- 

Tropical Cyclones [View project](#)



## The role of mangroves in attenuating storm surges

Keqi Zhang<sup>a,b,\*</sup>, Huiqing Liu<sup>b</sup>, Yuepeng Li<sup>b</sup>, Hongzhou Xu<sup>b</sup>, Jian Shen<sup>c</sup>, Jamie Rhome<sup>d</sup>, Thomas J. Smith III<sup>e</sup>

<sup>a</sup> Department of Earth and Environment, Florida International University, 11200 SW 8th Street, Miami, FL 33199, USA

<sup>b</sup> International Hurricane Research Center, Florida International University, 11200 SW 8th Street, Miami, FL 33199, USA

<sup>c</sup> Virginia Institute of Marine Science, College of William & Mary, Gloucester Point, VA 23062, USA

<sup>d</sup> National Hurricane Center, Storm Surge Unit, 11691 SW 17th St, Miami, FL 33165, USA

<sup>e</sup> U.S. Geological Survey, Southeast Ecological Science Center, 600 Fourth Street South, St. Petersburg, FL 33701, USA

### ARTICLE INFO

#### Article history:

Received 22 February 2012

Accepted 23 February 2012

Available online 7 March 2012

#### Keywords:

storm surges

mangroves

bioshields

Hurricane Wilma

surge modeling

### ABSTRACT

Field observations and numerical simulations indicate that the 6-to-30-km-wide mangrove forest along the Gulf Coast of South Florida effectively attenuated storm surges from a Category 3 hurricane, Wilma, and protected the inland wetland by reducing an inundation area of 1800 km<sup>2</sup> and restricting surge inundation inside the mangrove zone. The surge amplitude decreases at a rate of 40–50 cm/km across the mangrove forest and at a rate of 20 cm/km across the areas with a mixture of mangrove islands with open water. In contrast, the amplitudes of storm surges at the front of the mangrove zone increase by about 10–30% because of the “blockage” of mangroves to surge water, which can cause greater impacts on structures at the front of mangroves than the case without mangroves. The mangrove forest can also protect the wetlands behind the mangrove zone against surge inundation from a Category 5 hurricane with a fast forward speed of 11.2 m/s (25 mph). However, the forest cannot fully attenuate storm surges from a Category 5 hurricane with a slow forward speed of 2.2 m/s (5 mph) and reduced surges can still affect the wetlands behind the mangrove zone. The effects of widths of mangrove zones on reducing surge amplitudes are nonlinear with large reduction rates (15–30%) for initial width increments and small rates (<5%) for subsequent width increments.

© 2012 Elsevier Ltd. All rights reserved.

### 1. Introduction

One of the ecologic services providing by mangroves is to buffer the impacts of waves, storm surges, and tsunamis on coastal property and infrastructure by dissipating incoming wave energy (Barbier et al., 2008; Cochard et al., 2008). The role of mangroves in attenuating short-period wave energy has been well documented by theoretical analysis and field observations (Mazda et al., 1997; Möller et al., 1999). However, conclusions regarding mangrove effects on long waves, including storm surges and tsunamis, are controversial (Danielsen et al., 2005; Dahdouh-Guebas, 2006; Kerr and Baird, 2007; Cochard et al., 2008; Feagin, 2008; Baird et al., 2009; Das and Vincent, 2009; Tanaka, 2009; Feagin et al., 2010). Previous studies on the protective function of mangroves against storm surges and tsunamis are mainly based on statistical analysis of the relationship between locations and sizes of mangrove forests and

damage to built structures through after-event surveys (Kathiresan and Rajendran, 2005; Chatenoux and Peduzzi, 2007; Iverson and Prasad, 2007; Olwig et al., 2007; Das and Vincent, 2009). However, the reliability of statistical analysis is limited by the difficulty in separating multiple, correlated, spatially varying variables, such as heights of inundation water levels, topographic elevations, distances to the shoreline, and sizes of mangrove forests. The numerical simulations of tsunami inundation were only conducted for coastal areas having small areas of mangrove forests (Hiraishi and Harada, 2003; Yanagisawa et al., 2009), and their reliability is in question due to lack of high quality topographic and bathymetric data.

The major reason for the debate on the protective function of mangroves is that no systematic field measurements of storm surge and tsunami in mangrove forests were available except for one recent study (Krauss et al., 2009; Feagin et al., 2010). In this recent study, Krauss et al. (2009) analyzed water level data recorded inside the mangrove zone at the Gulf Coast of South Florida during Hurricanes Charley (2004) and Wilma (2005) to show that mangroves could reduce storm surge heights as much as 9.4 cm/km. However, surge measurements at the ocean front of the mangrove zone are missing in the dataset of Krauss et al. thus, their analysis of surge

\* Corresponding author. Department of Earth and Environment, Florida International University, 11200 SW 8th Street, Miami, FL 33199, USA

E-mail address: [zhangk@fiu.edu](mailto:zhangk@fiu.edu) (K. Zhang).

decay over the mangrove forest is incomplete. Furthermore, no previous studies have provided answers to the following questions that are essential to determine the role of mangrove forests as bio-shields against storm surges: (1) What is the difference in the inundation process with and without mangroves? (2) How does surge amplitude decay across a mangrove zone? (3) What is the alongshore change of surge inundation across mangrove zones? (4) What is the threshold size of mangrove forests beyond which surge heights are reduced significantly for a given category of hurricane? We address these questions by analyzing abundant field measurements of the storm surge from Hurricane Wilma and performing numerical simulations based on highly accurate topographic data from airborne light detection and ranging (LiDAR) measurements. The structure of the remainder of this paper is arranged as follows: Section 2 depicts the study area, describes Hurricane Wilma and field measurements of storm surges, and presents digital elevation models (DEMs) from LiDAR surveys and other sources; Section 3 presents the Coastal and Estuarine Storm Tide (CEST) Model and settings; Section 4 is a description for the simulation of storm surge from Wilma and model verification; Section 5 examines the effect of mangrove sizes and the effect of hurricane intensity and moving speed on surge reduction; Section 6 is for discussions; Section 7 draws conclusions.

## 2. Setting of the study area and data

### 2.1. Study area

The examination of the hypothesis whether mangroves significantly attenuate storm surges requires a low-lying coastal area characterized by wide mangrove zones and high storm surges. The Gulf Coast of South Florida from Sanibel Island to Key West is

a study area that satisfies these requirements (Fig. 1). The funnel-shaped shoreline and a large area of shallow water often lead to high storm surges when a hurricane makes landfall at the upper Gulf Coast of the study area. Additionally, South Florida is one of the world's most vulnerable areas to inundation caused by storm surge due to its gently-sloped topography with vast areas only a few meters above the current sea level (Zhang, 2011).

The mangrove forest in South Florida, which is the largest in the United States, is mainly distributed along the southwest coast of Florida next to the Gulf of Mexico and the south coast adjacent to Florida Bay, covering a coastline of 200 km and an area of 2800 km<sup>2</sup> (Fig. 1). The width of the mangrove zone varies from 6 to 30 km along the coast, depending upon topography, the range of tidal flooding, and the amount of freshwater from the Everglades. Tall mangrove trees with heights of 4–18 m and stem diameters of 5–60 cm occupy the Gulf Coast and the west portion of the northern Florida Bay Coast, while scrub mangroves with heights less than 4 m are distributed further inland (Simard et al., 2006). The dominant species of the forest are *Rhizophora mangle*, *Laguncularia racemosa*, and *Avicennia germinans*. The topography at the mangrove zone is nearly flat with elevations near 0 m referenced to NAVD88. The mangrove forest is not directly impacted by the recent urbanization because of the protection offered by Everglades National Park. The mangroves are frequently impacted by storm surges and high winds from hurricanes because South Florida is subject to tropical storms from both the Atlantic Ocean and the Gulf of Mexico, but most mangrove forests recover through advanced or seedling regeneration (Ward et al., 2006). Prior to 2005, the most recent storm to catastrophically impact the mangrove zone in South Florida was Andrew in 1992, and the effects of surge and wind on mangrove forest have been minimized through a more than ten-year recovery.

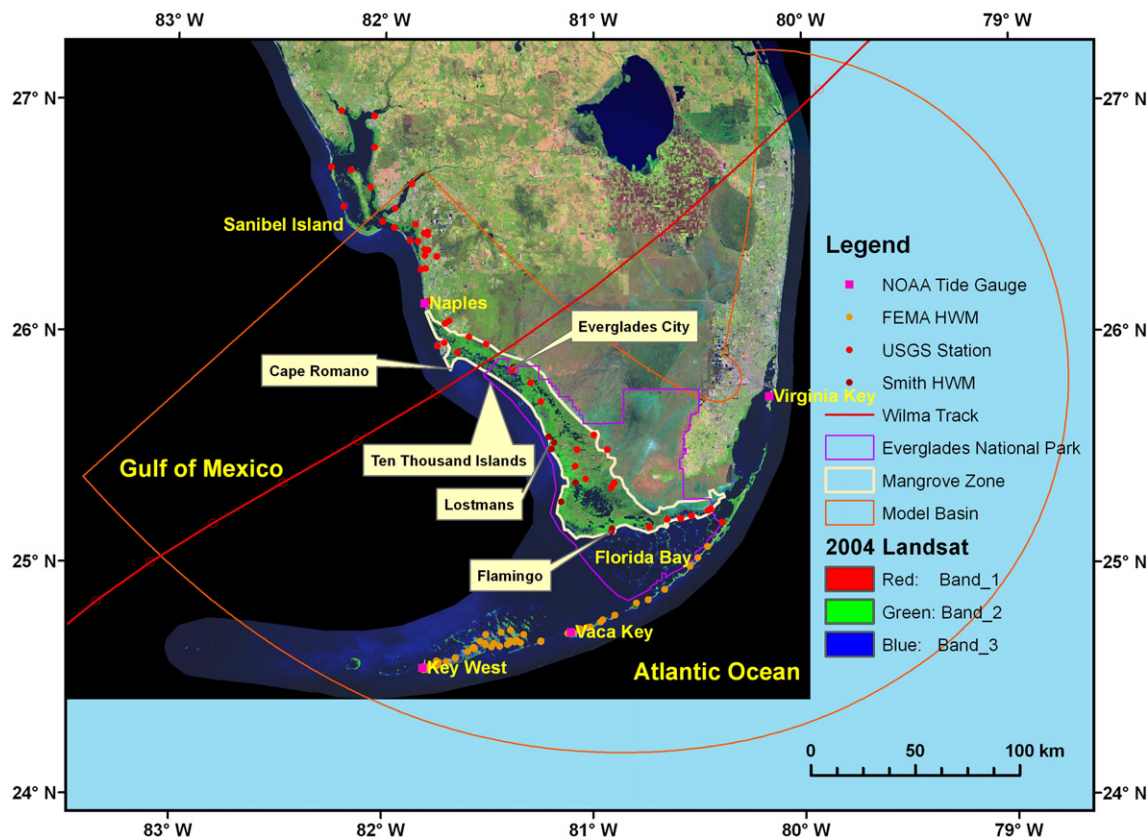


Fig. 1. The study area, the CEST model basin, and locations of storm surge measurements.

## 2.2. Hurricane Wilma and storm surge measurements

Hurricane Wilma, advancing toward the South Florida Peninsula from the Gulf of Mexico, made landfall as a Category 3 hurricane between Everglades City and Cape Romano around 10:30 coordinated universal time (UTC) on 24 October 2005 (Fig. 1). With an extraordinarily wide eye of 89–105 km in diameter and a track at the upper Gulf Coast of the study area, Wilma resulted in extensive coastal inundation with a maximum storm surge of 5 m (Smith et al., 2009).

Abundant storm surge measurements for Hurricane Wilma were collected along the South Florida Coast by various agencies, including the National Oceanic and Atmospheric Administration (NOAA), the U.S. Geological Survey (USGS), the Federal Emergency Management Agency (FEMA), and academic researchers (Fig. 1). NOAA maintains several tide gauges along the South Florida coast that measure water level changes continuously (National Ocean Service, 2005). USGS has set up a large number of water level gauges in small rivers and tidal creeks in Everglades National Park to monitor the hydro-period of the freshwater flows (Telis, 2006). The gauges in the estuaries along the Gulf Coast and Florida Bay captured the signal of storm surges from Wilma. In addition, USGS has deployed dozens of mobile gauges in rivers and creeks, mostly along the Gulf Coast, to collect storm surge inundation data (Soderqvist and Byrne, 2007). FEMA collected about 50 high water mark elevations using GPS surveys along the Florida Keys through a subcontract to URS Group Inc. (FEMA and URS Group Inc., 2006). USGS and academic researchers who monitor the changes of the mangrove forest in Everglades National Park collected water level records, high water mark measurements, and thickness of surge sediment inside the mangrove zone during and after Wilma (Krauss et al., 2009; Smith et al., 2009; Castañeda-Moya et al., 2010). Therefore, a rich array of field measurements of surges from Wilma allow us to validate the surge model and examine spatial changes in the interaction between surges and mangroves.

## 2.3. LiDAR DEM and shoreline

Local topographic features, such as coastal ridges, barrier islands, and sand dunes, have a great effect on the process and extent of overland flooding. The accurate simulation of surge inundation relies upon high-resolution topographic data. The 12,400 km<sup>2</sup> of LiDAR data that cover the coastal areas vulnerable to storm surge flooding in South Florida were collected in 2007 by the Florida Division of Emergency Management. Based on the comparison between LiDAR data with ground control points, the average vertical root-mean-square (RMS) error of the LiDAR data is less than 0.15 m, which corresponds to a vertical accuracy better than 0.30 m at the 95% confidence level. DEMs for South Florida with a horizontal resolution of 8 m were generated by the South Florida Water Management District (SFWMD) by interpolating identified terrain LiDAR measurements using the triangulated irregular network (<http://www.sfwmd.gov>). In addition, elevation measurements collected by USGS using an airborne height finder (AHF) were used to generate the DEM for an area of 10,800 km<sup>2</sup> in the Everglades (Desmond, 2003), where the remote sensing technology such as aerial photogrammetry and LiDAR is not effective in mapping the elevations of the areas covered by turbid water and vegetation. The AHF elevation points were interpolated into a 30 × 30 m DEM using the Kriging method in ArcGIS ([www.esri.com](http://www.esri.com)). A digital shoreline provided by the Florida Division of Emergency Management was also used to separate land and ocean cells of the CEST model grid. The shoreline depicts boundaries of land and islands (>2 km<sup>2</sup>) embedded within water bodies.

## 3. The CEST storm surge model and settings

### 3.1. Hydrodynamic model

The CEST model, operating in a depth-integrated, two dimensional (2D) form over an orthogonal curvilinear grid, was employed to simulate Wilma's surge (Zhang et al., 2008b). The 2D depth-integrated continuity equation in an  $x$ ,  $y$ , and  $z$  coordinate system with the  $z$ -axis perpendicular to the still water level is:

$$\frac{\partial \zeta}{\partial t} + \frac{\partial HU}{\partial x} + \frac{\partial HV}{\partial y} = 0 \quad (1)$$

and the momentum equations along the  $x$  and  $y$  directions are:

$$\begin{aligned} \frac{\partial HU}{\partial t} + \frac{\partial HU^2}{\partial x} + \frac{\partial HUV}{\partial y} = fHV - g \frac{\partial}{\partial x} \left( \zeta + \frac{\Delta P_a}{\rho g} \right) - \frac{\tau_b^x}{\rho} + \frac{\tau_s^x}{\rho} \\ + A_h \frac{\partial^2 HU}{\partial x^2} + A_h \frac{\partial^2 HU}{\partial y^2} \end{aligned} \quad (2)$$

$$\begin{aligned} \frac{\partial HV}{\partial t} + \frac{\partial HUV}{\partial x} + \frac{\partial HV^2}{\partial y} = -fHU - g \frac{\partial}{\partial y} \left( \zeta + \frac{\Delta P_a}{\rho g} \right) - \frac{\tau_b^y}{\rho} + \frac{\tau_s^y}{\rho} \\ + A_h \frac{\partial^2 HV}{\partial x^2} + A_h \frac{\partial^2 HV}{\partial y^2} \end{aligned} \quad (3)$$

where,  $H$  is the water depth from the still water level to the bottom,  $\zeta$  is the water surface elevation reference to the still water level,  $U$  and  $V$  are depth-integrated velocities along the  $x$  and  $y$  directions,  $f$  is the Coriolis parameter,  $g$  is the gravitational acceleration,  $\Delta P_a$  is air pressure drop,  $\rho$  is the water density,  $A_h$  is the horizontal eddy diffusivity. The bottom friction forces  $\tau_b^x$  and  $\tau_b^y$  are given by a quadratic drag law:

$$\tau_b^x = \rho C_b \sqrt{U^2 + V^2} U \quad (4)$$

$$\tau_b^y = \rho C_b \sqrt{U^2 + V^2} V \quad (5)$$

where  $C_b$  is the coefficient based on the Chezy formula:

$$C_b = \frac{gn^2}{H^{1/3}} \quad (6)$$

where  $n$  is the Manning coefficient. The surface wind stresses  $\tau_s^x$  and  $\tau_s^y$  are given by a similar formulation:

$$\tau_s^x = \rho_a C_s \sqrt{(U_a - U)^2 + (V_a - V)^2} (U_a - U) \quad (7)$$

$$\tau_s^y = \rho_a C_s \sqrt{(U_a - U)^2 + (V_a - V)^2} (V_a - V) \quad (8)$$

where  $\rho_a$  is the air density and  $U_a$ ,  $V_a$  are the wind velocities at the 10-m height above the still water level along the  $x$  and  $y$  directions.  $C_s$  is the drag coefficient based on the formula of Large and Pond (1981) and Powell et al. (2003).

$$C_s = \begin{cases} 0.00114 & \sqrt{U_a^2 + V_a^2} \leq 10 \\ \left( 0.49 + 0.0065 \sqrt{U_a^2 + V_a^2} \right) 10^{-3} & 10 < \sqrt{U_a^2 + V_a^2} \leq 38 \\ 0.003 & \sqrt{U_a^2 + V_a^2} > 38 \end{cases} \quad (9)$$

The 2D CEST model is discretized on an orthogonal curvilinear grid based on the modified C-grid with velocity components on the four edges of a grid cell and the water depths at the center and four



edges (Zhang et al., 2008b). A mass balanced wetting and drying algorithm involving the accumulated water volume within a grid cell is employed to compute the flood and ebb storm surge over the land.

### 3.2. Wind field computation

Both parametric models and time series of wind fields (H\*Wind) generated by the Hurricane Research Division of NOAA based on field measurements (Powell et al., 1998; Houston et al., 1999) can be used to compute wind stresses. The parametric wind model used by the Sea, Lake, and Overland Surge from Hurricane (SLOSH) model (Jelesnianski et al., 1992) was employed to estimate the hurricane wind field when H\*Wind data were not available. To account for the terrain effect on the wind, two different drag coefficients are used to compute the wind field on the terrain and extreme shallow waters and the wind field on the ocean, which are referred to as lake wind and ocean wind, respectively. The effects of vegetation on the wind field have also been accounted for in a way similar to the SLOSH model. The wind speed is adjusted using a coefficient  $C_T$  based on the ratio of the surge water depth ( $D = H + \zeta$ ) to the vegetation height ( $H_T$ ):

$$C_T = \begin{cases} \frac{D}{H_T} & D < H_T \\ 1 & D \geq H_T \end{cases} \quad (10)$$

The effect of trees on the wind speed decreases based on this equation as the water submerges the vegetation gradually. In this study, the land areas covered by dense vegetation and development were classified into the “Tree” category and assigned an average vegetation height of 8 m, the same as the one used by SLOSH for the Florida Keys basin. When a storm surge floods low-lying areas, it often forms a thin layer of water over land. An extinction coefficient  $C_E$  is applied to the wind speed to reduce its effect on the thin layer of water (Jelesnianski et al., 1992).

$$C_E = \begin{cases} \frac{D}{0.3} & D < 0.3\text{m} \\ 1 & D \geq 0.3\text{m} \end{cases} \quad (11)$$

### 3.3. Model grid and water depth calculation

The model domain includes the Gulf and Atlantic Coasts of South Florida, Florida Bay, and Florida Keys. The model grid, comprised of approximately 110,000 cells, extends from 78.7°W to 83.4°W in longitude and from 24.2°N to 27.2°N in latitude (Fig. 1). Resolutions of grid cells range from 700 × 850 m near the coast to 1300 × 1600 m at the open ocean. Water depths for grid cells at the open ocean were interpolated from the ETOPO1 global relief dataset from NOAA, which has a resolution of 1 arc minute (1.5–2 km). Water depths for grid cells in coastal areas were interpolated from the U.S. coastal relief dataset from NOAA with a resolution of 3 arc second (90 m) ([http://www.ngdc.noaa.gov/mgg/gdas/gd\\_designagrid.html](http://www.ngdc.noaa.gov/mgg/gdas/gd_designagrid.html)). Both relief datasets were adjusted to the NAVD88 vertical datum before interpolation.

Topographic elevations for land cells were computed using 30 × 30 m USGS, 8 × 8 m LiDAR, and 30 × 30 m AHF DEMs for South Florida. First, the land cells of the model grid were identified by clipping the shapefile that consists of model cell polygons using a land boundary polygon in ArcGIS. Then, an area weighted, average elevation was calculated based on elevations of non-overlapped DEM pixels from LiDAR, AHF, and USGS. There is little overlap between LiDAR and AHF measurements. When USGS DEMs overlap

with LiDAR or AHF DEMs, only LiDAR or AHF DEMs were used to calculate the average elevation.

### 3.4. Drag and bottom friction force calculation

Vegetation such as mangroves not only reduces the hurricane wind by increasing surface roughness, but also affects the overland surge flow. The effects of emergent vegetation on the water flow can be accounted for by the drag force (Nepf, 1999; Mazda et al., 2005):

$$\tau_D = \frac{1}{2} C_D \rho A u |u| \quad (12)$$

where  $u$  is the water velocity,  $A$  is the projected plant areas perpendicular to  $u$ , and  $C_D$  is the drag coefficient. Since both drag and bottom friction forces have a quadratic relationship with the water velocity, the drag force can be included into the bottom friction force by adding an additional item into the Manning coefficient, assuming that there is no interaction between drag and bottom friction forces (Petryk and Bosmajian, 1975; Green, 2005; Wamsley et al., 2010). Since few spatial data for species abundance, stem sizes, and canopy structures are available for delineating subtle changes of Manning coefficients within the mangrove zone in the study area, a constant Manning coefficient was employed for mangrove trees in surge simulation. Sensitivity analysis from a previous study (Xu et al., 2010) showed that a Manning value of 0.15 for a dense mangrove area generated simulations matching with observed inundation boundaries. There are numerous lakes, rivers, and creeks inside the mangrove zone in the study area, therefore, the Manning coefficient for mangrove was reduced to 0.14.

The spatial coverage of mangrove forests in the study area was derived from the national land cover dataset (NLCD) created by USGS in 2001 (Homer et al., 2004). NLCD does not distinguish the mangrove forest from other coastal woody wetlands. In a comparison with the land cover dataset created by digitizing high-resolution aerial photographs collected in 2004 by SFWMD, the area of woody wetlands delineated in NLCD is almost identical to the mangrove zone in the SFWMD dataset. Considering that NLCD covers the entire model basin and is in an easy to process raster format, the coastal woody wetland areas in NLCD were used to represent mangrove zones along the Gulf Coast of South Florida. In addition to mangrove trees, other types of vegetation such as marsh grasses and buildings can also reduce the water flow. The effects of land cover on surge water flow are considered by introducing various Manning coefficients based on NLCD. A modified table of Manning coefficients (Table 1) corresponding to different land cover categories proposed by Mattocks and Forbes (2008) was employed in this study. The spatial resolution of NLCD, which were generated based on Landsat satellite imagery, is 30 m. This resolution is much higher than the cell size of the CEST model, which is about 700 × 850 m along the Gulf Coast of South Florida. Therefore, an average Manning coefficient ( $n_a$ ) for a grid cell was calculated using:

$$n_a = \frac{\sum_{i=1}^N (n_i \alpha) + n_0 \beta}{N \alpha + \beta} \quad (13)$$

where  $n_i$  is the Manning coefficient values of an NLCD pixel within a model grid cell,  $\alpha$  is the area of an NLCD pixel,  $N$  is the total number of NLCD pixels within a model cell,  $n_0$  is the constant Manning coefficient, 0.02, for the area  $\beta$  that is covered by ocean water, but not covered by NLCD pixels. Fig. 2 shows that large Manning coefficients occur along the Gulf Coast of South Florida in the model basin, especially in the coastal zone with mangroves,

**Table 1**

Manning coefficients for various categories of land cover (modified from Mattocks and Forbes, 2008).

NLCD Class number	NLCD Class name	Manning coefficient
11	Open water	0.020
12	Perennial ice/Snow	0.010
21	Developed open space	0.020
22	Developed low intensity	0.050
23	Developed medium intensity	0.100
24	Developed high intensity	0.130
31	Barren land (Rock/Sand/Clay)	0.090
32	Unconsolidated shore	0.040
41	Deciduous forest	0.100
42	Evergreen forest	0.110
43	Mixed forest	0.100
51	Dwarf scrub	0.040
52	Shrub/Scrub	0.050
71	Grassland/Herbaceous	0.034
72	Sedge/Herbaceous	0.030
73	Lichens	0.027
74	Moss	0.025
81	Pasture/Hay	0.033
82	Cultivated crops	0.037
90	Woody wetlands	0.140
91	Palustrine forested wetland	0.100
92	Palustrine scrub/Shrub wetland	0.048
93	Estuarine forested wetland	0.100
94	Estuarine scrub/Shrub wetland	0.048
95	Emergent herbaceous wetlands	0.045
96	Palustrine emergent wetland (Persistent)	0.045
97	Estuarine emergent wetland	0.045
98	Palustrine aquatic bed	0.015
99	Estuarine aquatic bed	0.015

while the Atlantic Coast, which is covered by developments and marshes, has smaller Manning coefficients. The Manning coefficient of the ocean bottom was set to be a constant value of 0.02.

### 3.5. Boundary and initial conditions

The tides were not included in the simulations because of small tide ranges (0.3–0.6 m) in the study area (He and Weisberg, 2002). The partial clamped gravity wave radiation open boundary condition (Blumberg and Kantha, 1983) was used at the open boundaries:

$$\frac{\partial \zeta}{\partial t} + C \frac{\partial \zeta}{\partial n} = - \left( \frac{\zeta - \zeta_k}{T_f} \right) \quad (14)$$

where  $C = \sqrt{gH}$  is the phase speed of the long wave and  $n$  is the direction normal to the planar boundary. The damping term on the right side of the equation tends to reduce the value  $\zeta$  at the boundary to the known value  $\zeta_k$  with a time scale on the order of  $T_f$ .  $\zeta_k$  and  $T_f$  are set to be 0 m and 7.2 h in this study based on numerical experiments. The mean values of water levels from 1 October to 23 October 2005, prior to Wilma, at NOAA's Naples, Key West, Vaca Key, and Virginia Key tide gauges, which are scattered inside the model domain (Fig. 1), range from 0.01 to 0.07 m above the NAVD88 datum, with an average value of 0.04 m. Therefore, the still water levels at the initial stage for surge simulations was set to be the same as the NAVD88 datum by neglecting this small difference.

## 4. Simulation of Wilma's surge and model verification

Four simulations of Wilma's surges were conducted in order to examine the effects of wind field and land cover on storm surges and verify the CEST model. The first simulation used SLOSH wind

and constant Manning coefficients of 0.02 for all grid cells. The second simulation used the SLOSH wind and varying Manning coefficients for land cells based on NLCD. The third simulation used H\*Wind and constant Manning coefficients of 0.02, while the fourth simulation used H\*Wind and the NLCD-based Manning coefficients. Each simulation, starting at 14:00 UTC on 21 October 2005 and ending at 18:00 UTC on 25 October, continued for 100 h with a time step of 60 s. In order to examine the effect of grid resolution on simulations, we have also conducted surge simulations over the grid with a cell size of  $230 \times 280$  m at the coastal area that was generated by refining the original grid three times. The comparisons of computed surge amplitudes and inundation extents for these four cases show that there is little difference between the simulations for two different grids. Since the computation time for the refined grid is about 50 times of that for the original grid, the numerical experiments in Section 5 were only performed over the original grid and only the results for the original grid were presented.

A comparison of observed peak surge heights (surge amplitudes) with those computed using the SLOSH wind and constant Manning coefficients shows a considerable scatter with an RMS error of 0.63 m (Fig. 3a). By incorporating the effects of land cover (Fig. 3b), the RMS error of computed peak surge heights versus observed ones decreases from 0.63 m to 0.47 m, about 24% less. The effects of mangrove trees on storm surge inundation are more obvious when the RMS errors of peak surge heights in the Florida Keys, in the mangrove zone of the Gulf Coast, and in the Gulf coastal area without mangrove trees are compared separately (Table 2). The RMS error of computed peak surge heights in the Florida Keys does not change much between cases with and without incorporating the effects of land cover. In contrast, the variability of computed versus observed peak surge heights within the mangrove zone is much reduced by considering the tree effect in comparison to the variability seen without considering the tree effect. The RMS error decreases from 0.94 m to 0.47 m, about 50% less, indicating that mangroves have significant effects on surge simulation. The RMS error of computed peak surge heights in the Gulf coastal area without mangrove trees changes little between the two cases in which the effects of land cover are either ignored or included.

The computed peak surges versus observed ones for the H\*Wind-based simulation with land cover effects show much less variability than that for the simulation without land cover effects (Fig. 3c and d). The RMS error of computed peak surge heights is reduced from 0.60 m to 0.39 m by incorporating land cover effects, about 35% less than that without incorporating land cover effects. A detailed comparison of the RMS errors of H\*Wind-based simulations (Table 2) indicates that the incorporation of land cover effects changes peak surge simulations little in the Florida Keys, reduces the error of peak surge heights by 30% in the Gulf coastal area without mangrove trees, and dramatically improves the peak surge simulation in the mangrove zone by reducing the error by 59%. Both RMS errors of H\*Wind-based simulations with constant and NLCD-based Manning coefficients are smaller than those of the SLOSH wind-based simulations. The RMS error of peak surge heights from the simulation with H\*Wind and NLCD-based Manning coefficients is reduced from 0.47 to 0.39 m, compared to that from the simulation with the SLOSH wind and NLCD-based Manning coefficients. Note that the difference in peak surge heights in the presence and absence of land cover effects is larger than that caused by the disparity of the SLOSH wind and H\*Wind.

The inundation areas from the H\*Wind simulations are  $2450 \text{ km}^2$  and  $4220 \text{ km}^2$  with and without incorporating effects of land cover, indicating that mangroves also affect the inundation extent remarkably (Fig. 4). The simulated surges without land cover

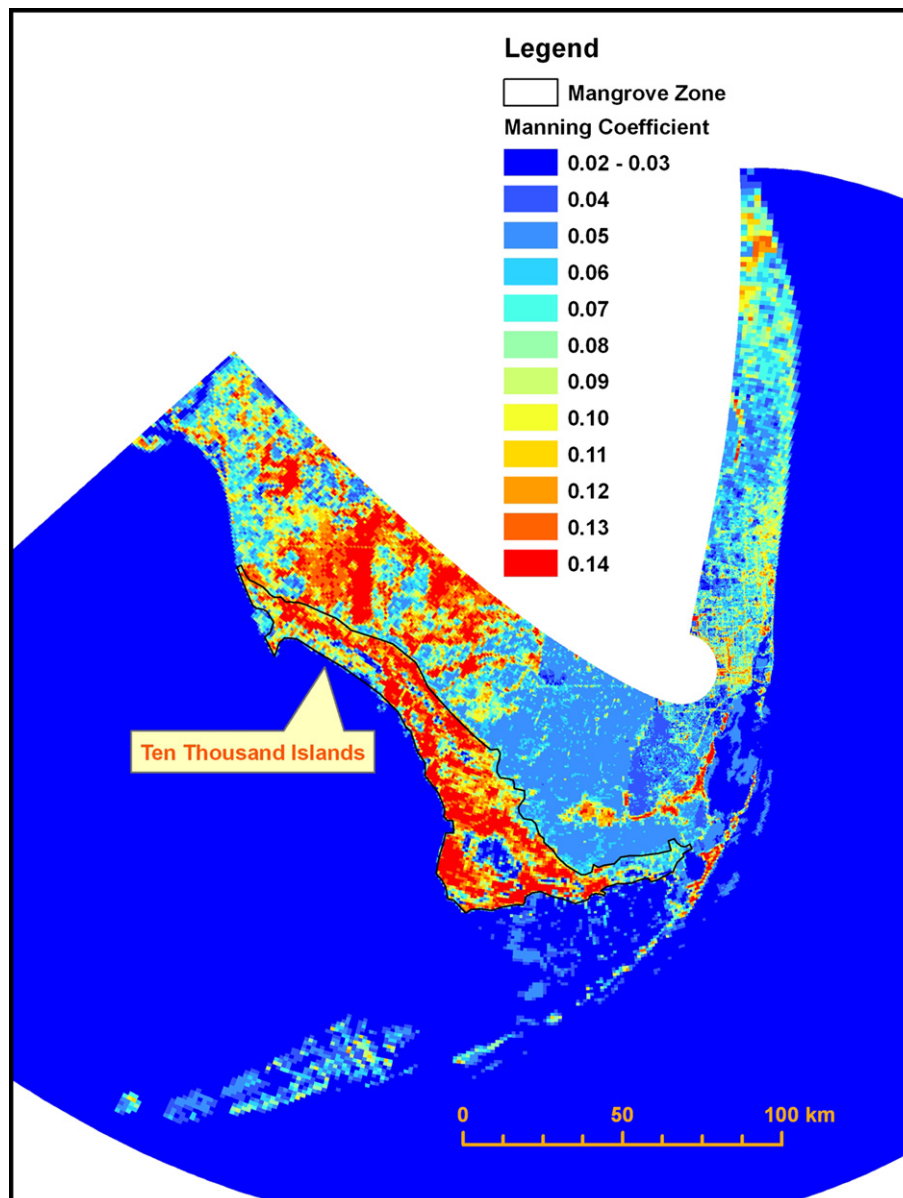


**Fig. 2.** Calculated Manning coefficients based on NLCD. Note that Manning coefficients are smaller along the coast of the Ten Thousand Islands due to less mangrove coverage, compared to the values at the coast south of the islands.

effects reach 13–40 km inland along four profiles, about 1–15 km beyond the mangrove zone. In contrast, the simulated inundation with land cover effects is restricted within the mangrove zone. Measurable surge-induced sediment deposits were found along a 70-km stretch of coastline from Lostmans River to Flamingo (Fig. 1), but were limited within a zone of less than 14 km from the Gulf of Mexico (Smith et al., 2009), providing a close agreement with the simulated inundation extents of 10–14 km when land cover effects are considered (Fig. 4b). Note that the dissipation of peak surge heights toward inland with land cover effects is much higher than that without the effects of land cover. The peak surge heights at the front of the mangrove zone increase by 10–30% compared to the peak surge heights there computed without incorporation of mangrove effects.

In summary, the comparison of computed and observed storm surges from Hurricane Wilma indicates that CEST replicates the magnitude and extent of overland flooding. The RMS error of computed versus measured peak surge heights is comparable to

those from other surge models (Bunya et al., 2010). The SLOSH wind and H\*Wind generate similar surge inundation patterns, with a slightly better result from H\*Wind overall. There are significant differences in simulated inundation extents and magnitudes with and without considering variations of Manning coefficients caused by spatial changes of land cover. The CEST model driven by H\*Wind or the SLOSH wind can be used to examine the effects of land cover including vegetation on storm surge inundation.

## 5. Sensitivity analysis of surge attenuation by mangroves

### 5.1. Effect of mangrove width on surge attenuation

The critical issue concerning the protective function of mangrove ecosystems against storm surges is to quantify the effect of mangrove zone width on surge attenuation. In order to estimate this effect, the mangrove zone was divided into 15 subzones starting from the shoreline with an increment of 1 km. Inside

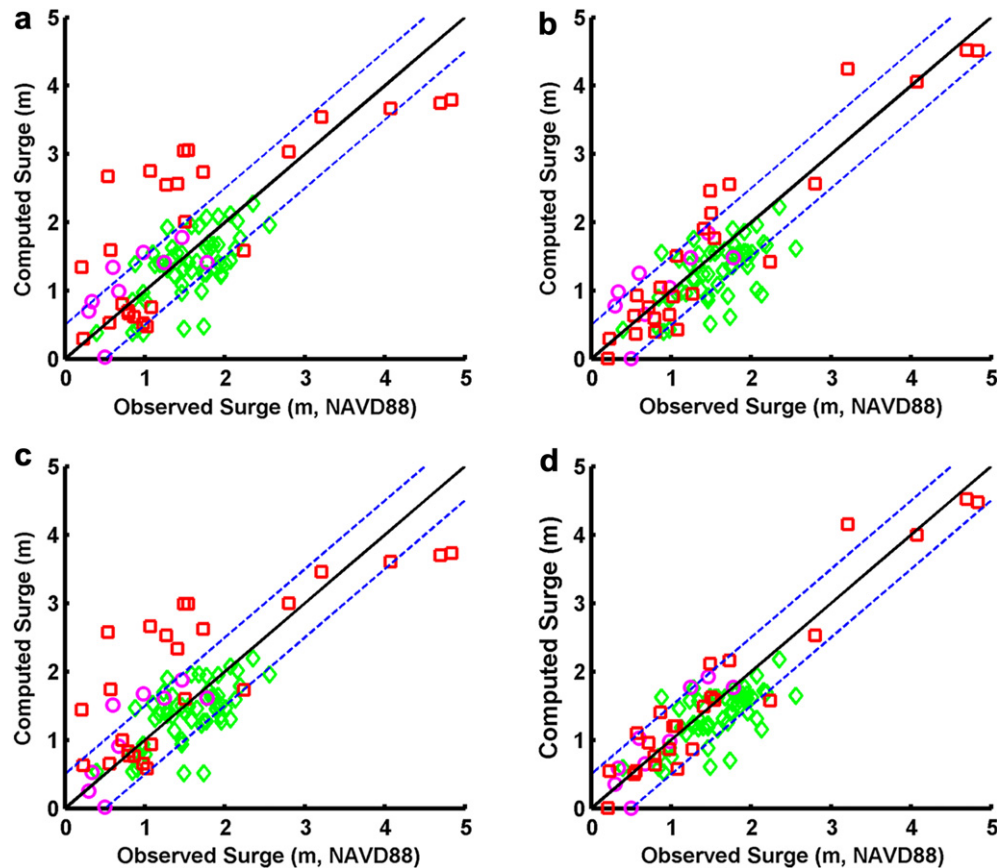


**Fig. 3.** Scatter plots of observed peak surge heights versus simulated ones generated (a) using SLOSH wind and constant Manning coefficients, (b) using the SLOSH wind and Manning coefficients based on NLCD, (c) using H\*Wind and constant Manning coefficients, and (d) using H\*Wind and Manning coefficients based on NLCD. The black line represents perfect simulations and the blue dashed lines represent the boundaries of perfect simulations  $\pm 0.5$  m. The green diamonds represent high water mark elevations in the Florida Keys collected by FEMA, the purple circles represent peak surge heights in the Gulf coastal area without mangroves collected by USGS, and the red squares represent peak surge heights in the mangrove zone collected by USGS and Smith et al. (2009). Both computed and observed peak surge heights are referenced to the NAVD88 vertical datum. The high water mark elevations in Smith's dataset that were originally referenced to the ground surface were converted to be in NAVD88 using ground elevations derived from a  $3 \times 3$  m LiDAR DEM. Only observed surge points inundated by all four computed storm surges were used for comparison. Computed surges do not reach the locations with observed surges in some cases, especially when the gauges are located in rivers and creeks far inland. (For interpretation of the references to colour in this figure legend, the reader is referred to the web version of this article.)

subzones, the heights of trees were assigned values of 8 m for the wind field computation and Manning coefficients were calculated based on NLCD data. Outside subzones, tree heights and Manning coefficients were set to be 0 m and 0.02, respectively. Storm surge simulations were performed for 15 cases with Wilma's H\*Wind and varied widths of mangrove zones along the Gulf and Florida Bay Coasts of South Florida.

The results show that surge amplitudes, inundation extents, and surge decay patterns change remarkably as the width of the mangrove zone varies (Fig. 5). With a 1-km mangrove zone, surge amplitudes at the front of the mangrove zone increase by 3–18%

along four profiles (Fig. 4), compared to surge amplitudes there computed without mangroves. Surge amplitudes at the back of the mangrove zone are initially reduced drastically by 16–30%, compared to surge amplitudes at the front of the mangrove zone, and then exhibit a gradual decay pattern. With a 3-km mangrove zone, surge amplitudes increase and decrease by about 9–32% and 46–57%, respectively, at the front and back of the mangrove zone. With a 5-km mangrove zone, surge amplitudes at the back of the mangrove zone are reduced by 54–71%. Surge amplitudes at the front of the mangrove zone increase by 12–34%, changing little in comparison to surge amplitudes with a 3-km mangrove zone. With a 7-km mangrove zone, surge amplitudes at the back of the mangrove zone decrease by more than 72–86%, largely reducing the impact of storm surges to the ecosystems behind the mangrove zone. With a 10-km mangrove zone, surge amplitudes at the front and back of mangroves change little along the four profiles, compared to those of the 7-km mangrove zone. It appears that the threshold width of the mangrove zone for significant attenuation of the storm surge from Hurricane Wilma is about 7–8 km. This indicates that a mangrove zone with a width of several kilometers is needed to attenuate most of the storm surge from hurricanes like Wilma. Note that surge amplitudes at the front and back of the mangrove zone do not increase or decrease linearly as the mangrove zone becomes

**Table 2**  
RMS errors of computed versus measured peak surge heights.

Areas (Number of measurements)	SLOSH Wind with constant Manning (m)	SLOSH Wind with varying Manning (m)	H*Wind with constant Manning (m)	H*Wind with varying Manning (m)
Gulf coast with mangrove (25)	0.94	0.47	0.91	0.37
Gulf coast without mangrove (9)	0.46	0.42	0.47	0.33
Florida Keys Coast (53)	0.44	0.47	0.41	0.41
All coasts (87)	0.63	0.47	0.60	0.39



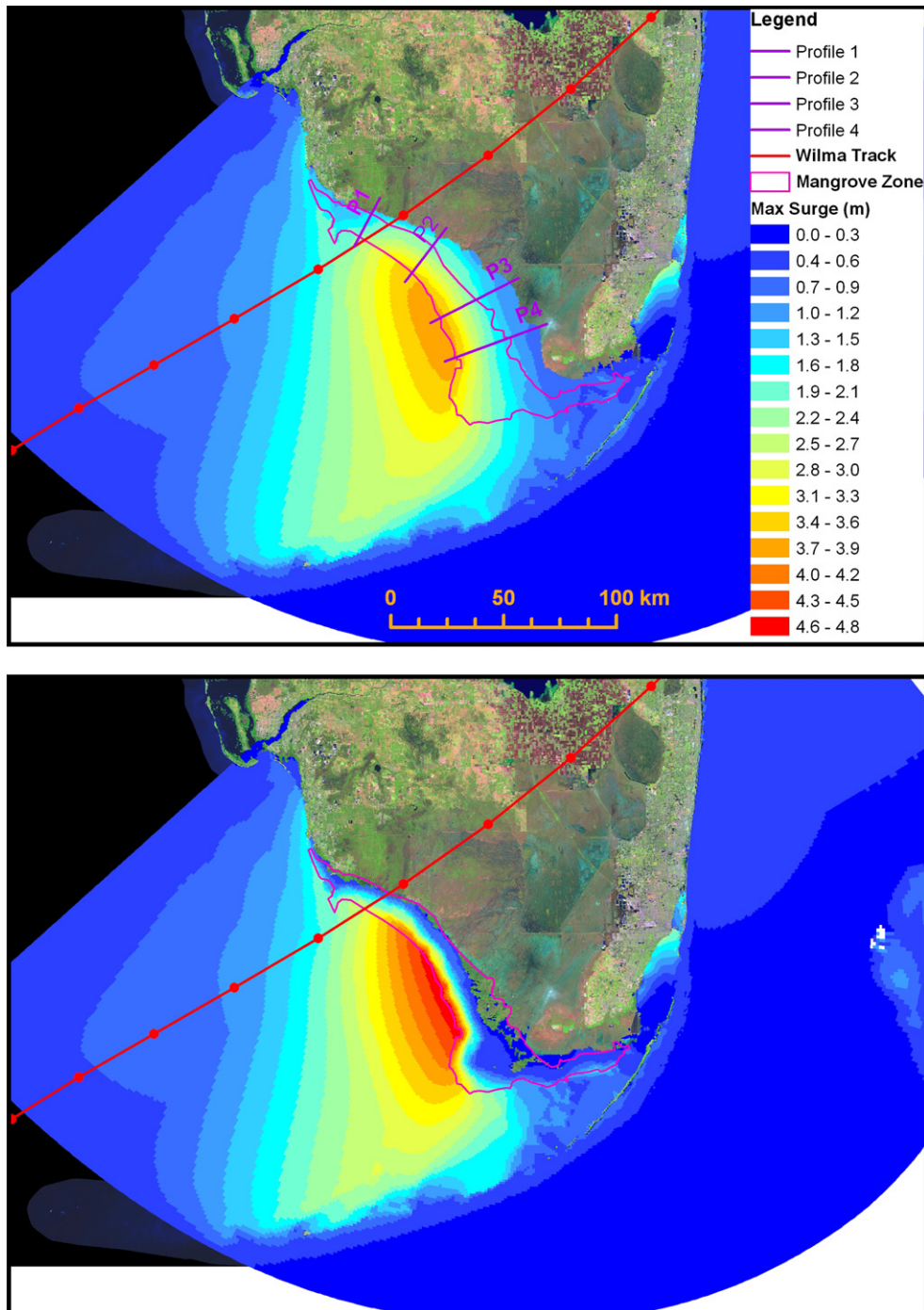


**Fig. 4.** Spatial distributions of computed peak surge heights using H\*Wind and constant Manning coefficients (upper plate) and using H\*Wind and Manning coefficients based on NLCD (lower plate). The solid circles along the hurricane track represent hourly center positions of Wilma. Peak surge heights are referenced to the NAVD88 vertical datum. The locations of four profiles in Figs. 5, 6 and 8 are also displayed.

wider. Large increases in peak surges at the front of mangrove zones occur when the widths of mangrove zones range from 1 to 3 km, while little change in peak surges at the front of mangrove zones occurs after the widths of mangrove zones are larger than 4 km. The surge reductions along Profiles 2, 3, and 4 have a similar nonlinear pattern, while Profile 1 shows relatively low initial surge reductions because of less coverage of mangroves (Fig. 6). Both reductions of surge amplitudes and inundation areas exhibit large initial rates and declining subsequent rates.

## 5.2. Effects of hurricane intensity and moving speed on surge attenuation

Three Category 4 and seven Category 3 hurricanes impacted the mangrove zone along the Gulf Coast of South Florida from 1851 to 2010, while no Category 5 hurricanes influenced the mangrove zone during this period (Zhang et al., 2008a). Although numerical simulations for three Category 4 hurricanes including the Labor Day Hurricane (1935), Donna (1960), and Andrew (1992)

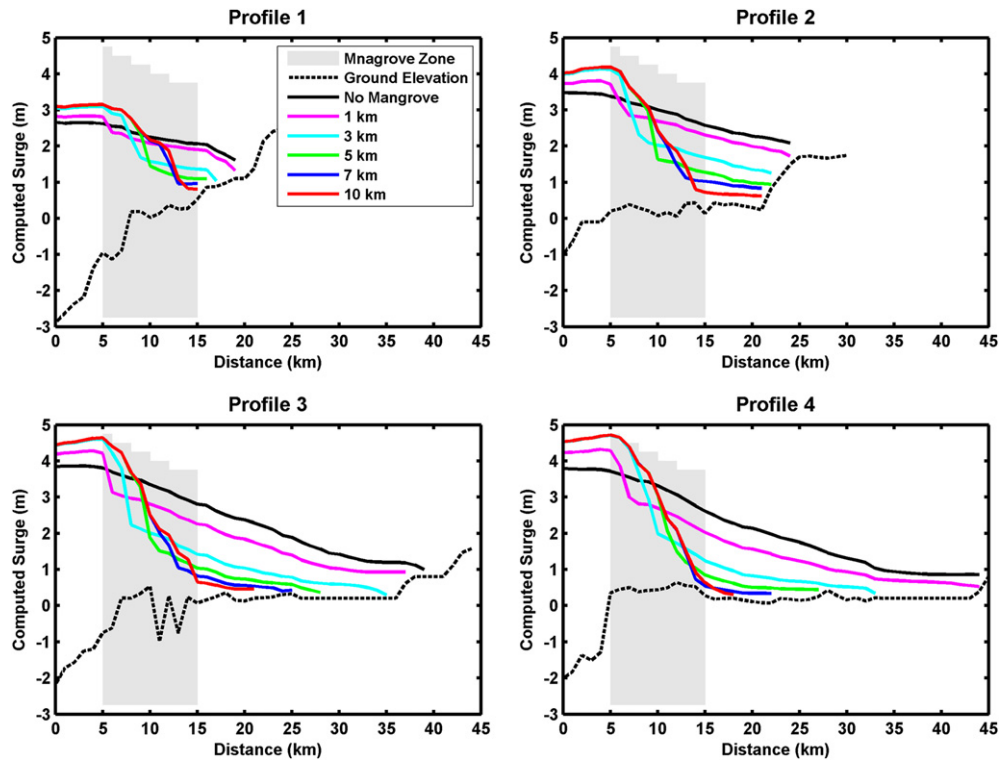


**Fig. 5.** The distributions of peak surge heights along four profiles across mangrove zones of varying widths. The gray area bars represent 1, 3, 5, 7, and 10 km widths of mangrove zones. The black dashed line depicts the elevations of a profile referenced to NAVD88. The black solid line represents surge amplitudes along a profile without mangrove effects, while other solid lines represent surge amplitudes along the profile with mangrove zones of varying widths. Note that surge amplitudes at the front of the mangrove zones are increased compared to the surge amplitude at the same location without the presence of mangroves. The large differences in surge amplitudes at the front and back side of a mangrove zone indicate that mangroves attenuate surge notably.

have not been conducted, the preliminary analysis based on field observations indicates that Wilma generated peak surge heights comparable to these three hurricanes (Smith et al., 2009) due to its large size and track position. Thus, storm surges from Wilma approximately represent a 40-year event for the mangrove zone along the Gulf Coast of South Florida. For these events, the current mangrove forest can provide an effective

protection of the freshwater marshes behind the mangrove zone from surge impacts. The question is whether the mangrove forest is effective against surges from more intense hurricanes.

In order to test the effects of hurricane intensity and moving speed on surge attenuation, Category 4 and 5 hurricanes with various forward speeds were employed to generate surges in comparison to those from Wilma. The National Hurricane Center generates synthetic hurricane tracks based on different intensities, forward speeds, and directions for each SLOSH basin in order to depict evacuation zones (Jelesnianski et al., 1992). Category 4 and 5 hurricanes with a 56-km (35-mile) radius of maximum wind for the Florida Keys were selected for testing. In order to compare simulated results with Wilma's surges, the tracks of Category 4 and 5 hurricanes with forward speeds of 2.2 m/s (5 mph), 6.7 m/s (15 mph), 11.2 m/s (25 mph) were projected onto Wilma's track first and then surge simulations were conducted.

The inundation extent of a rapidly moving Category 5 hurricane with a forward speed of 11.2 m/s is mostly restricted inside the mangrove zone (Fig. 7). In contrast, the storm water from a slowly moving Category 4 hurricane with a forward speed of 2.2 m/s passes through the mangrove zone and floods the large area at the back of the mangrove zone. The surge from a Category 5 hurricane with a forward speed of 2.2 m/s penetrates through the mangrove zone further, leading to 1.6–3.4 m surge amplitudes at the back of the mangrove zone depending upon the width of the mangrove zone (Figs. 7 and 8). Although the mangrove forest reduces surge amplitudes by 26–76%, surges can still impact the areas behind the mangrove zone because the wind has sufficient time to push the ocean water through the mangrove zone.

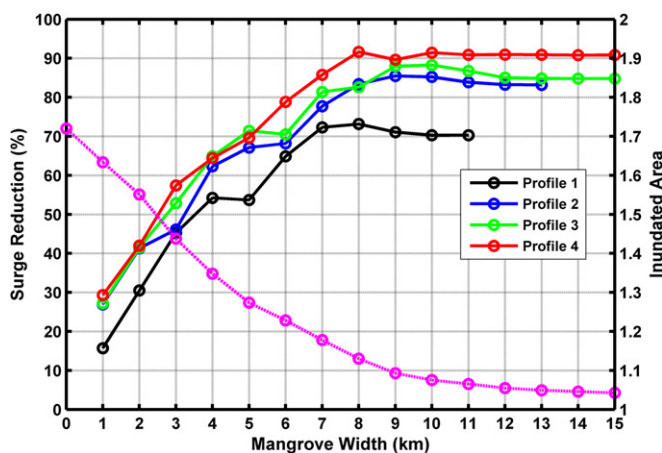


**Fig. 6.** The reduction of surge amplitude (solid lines) and decrease of inundated areas (dashed line) change as the width of the mangrove zone increases. The amplitude reductions in percentage were computed using the peak surge heights at the front and the back of the mangrove zone. The inundation areas inside and behind the mangrove zone were measured against the case when effects of mangroves and other land covers were considered.

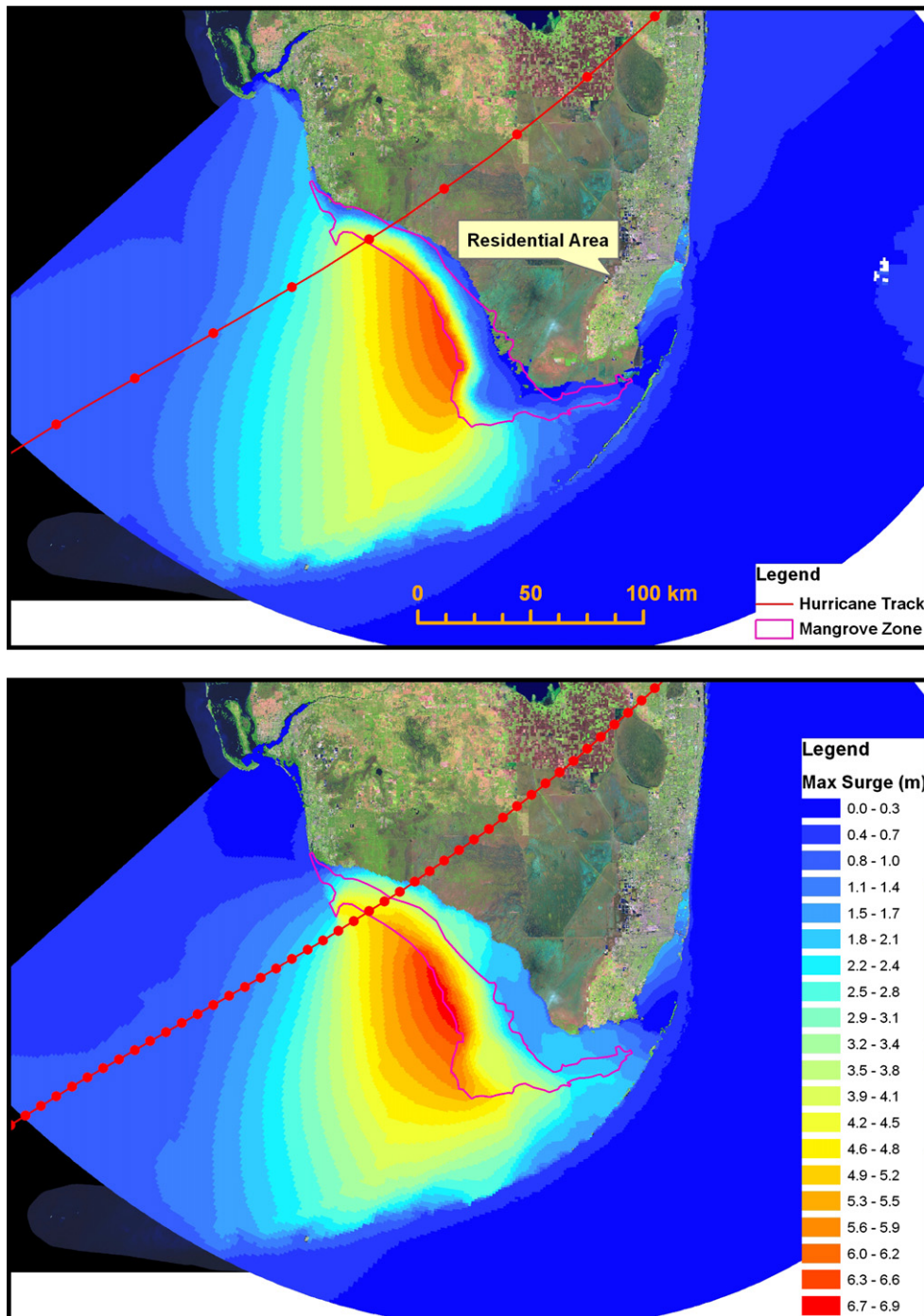


**Fig. 7.** Computed peak surge heights from a Category 5 hurricane with a forward speed of 11.2 m/s (25 mph) using the SLOSH wind and Manning coefficients based on NLCD (upper plate), and computed peak surge heights from a Category 5 hurricane with a forward speed of 2.2 m/s (5 mph) using SLOSH wind and Manning coefficients based on NLCD (lower plate).

## 6. Discussion

The decay rate of peak surge heights across the mangrove zone is an important index for measuring the effect of mangroves in reducing surge impacts. Estimates of the reduction rates of peak water levels for the wetlands along the Gulf Coast range from 4.2 to 18.9 cm/km according to the summary of previous studies provided by Krauss et al. (2009). However, these estimates were based on sparse field observations, and uncertainties of some earlier

estimates were not well documented. Also, the wetland types include both coastal marsh and forest; therefore, these estimates do not provide a consistent estimate for the peak water level reduction in mangrove zones. Based on water level records from the gauges inside the mangrove zone on the Gulf Coast of South Florida, Krauss et al. (2009) derived reduction rates of 4.2 cm/km for Wilma and 9.4 cm/km for Charley by fitting a linear equation to peak water levels. Calculations in Krauss et al. do not include surge amplitudes at the front of the mangrove zone, and therefore significantly



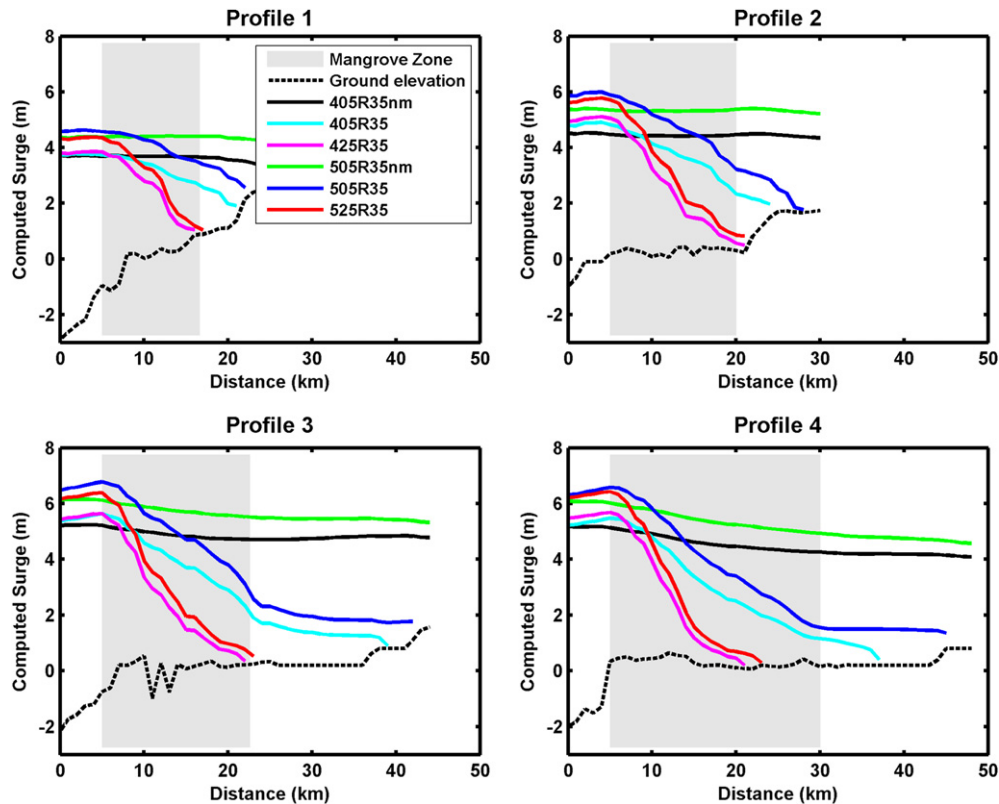


**Fig. 8.** The distributions of peak surge heights for synthetic Categories 4 and 5 hurricanes along four profiles across the mangrove zone at the Gulf Coast of South Florida. The gray area represents the mangrove zone. The legend 405R35 nm represents surge heights computed using a Category 4 hurricane with a 2.2 m/s (5 mph) forward speed and a 56-km (35-mile) radius of maximum wind without the mangrove effect. The legend 405R35 represents surge heights computed using a Category 4 hurricane with a 2.2 m/s (5 mph) forward speed and a 56 km (35 miles) radius of maximum wind with the mangrove effect. The legend 425R35 represents surge heights computed using a Category 4 hurricane with a 11.2 m/s (25 mph) forward speed and a 56-km (35-mile) radius of maximum wind with the mangrove effect. The legends 505R35 nm, 505R35, and 525R35 are for Category 5 hurricanes and represent the same features as those for Category 4 hurricanes.

underestimate the effect of mangrove forest on surge reduction. The utilization of water level records referenced to the ground surface, which are confounded with the variation in local topography, also increases the uncertainty of the estimation by Krauss et al. The surge amplitude decay rate across the mangrove zone for the first profile (Figure 4) is relatively low with a value of 23 cm/km because the drag force is reduced due to numerous open water areas in the Ten Thousand Islands area. The decay rates range from 40–48 cm/km for Profiles 2, 3, and 4 where there are fewer open water areas within the mangrove zone. These rates are almost one order of magnitude higher than the estimation of Krauss et al. at a similar location (Profile 4).

Statistical methods used to estimate the effect of mangroves on surge reduction explore the relationship between damage severity, physical variables such as bathymetric and topographic slopes, distances from the shore to impact areas, and surge amplitudes, as well as ecological variables such as the width of mangrove forest (Chatenoux and Peduzzi, 2007; Das and Vincent, 2009). Wilma's surge amplitudes decrease as they move inland even without vegetation effects, and decay rates change spatially as surge amplitudes decrease from their peak areas in both northerly and southerly directions along the shore (Figs. 4 and 5). It would be difficult to separate the influence of these factors from the mangrove effect on surge reduction based on sparse samples without additional information from numerical simulations. Therefore, it is not surprising to see that statistical analyses based on limited post-event surveys drew opposite conclusions (Baird et al., 2009; Das and Vincent, 2009). The appropriate way to

estimate the protective effects of coastal ecological systems on structures must combine sophisticated and well-calibrated numerical simulations with field observations.

The drag force upon water flow induced by mangroves is estimated by adding the drag coefficient to the Manning coefficient of the bottom friction in this study. Additionally, the effect of the variation of tree sizes inside the mangrove zone on surges is ignored by using a constant Manning coefficient for mangrove trees because it is difficult to accurately represent the drag coefficient influenced by roots, stems, and branches of mangrove trees in the water flow. The interaction of trees with the surge flow is a complicated process, which is related to species of mangroves, sizes of mangrove trees, and canopy structures of mangrove forests. For example, the *Rhizophora mangle* trees are more effective in dissipating the energy of low surges because of their dense stilt roots. The mangrove forest in the study area is comprised primarily of *Rhizophora mangle*, *Laguncularia racemosa*, and *Avicennia germinans* with varying abundance in space (Smith et al., 1994; Ward et al., 2006). The species, stem sizes, and densities of mangrove trees can be derived through field measurements (Ward et al., 2006), but the sparse field sample sites cannot capture the spatial changes of unevenly distributed species and stem sizes due to a cycle of growth, destruction, and regeneration caused by the disturbances from hurricanes and lightning strikes (Zhang et al., 2008a). The remote sensing technology such as radar and LiDAR provides an effective alternative for measuring tree heights in a large scale (Simard et al., 2006), but unfortunately, the density and species of mangrove trees cannot be derived directly from the



remote sensing data. However, it is reasonable to assume that the projected plant areas in the water flow direction is somewhat constant on average because mangrove tree stem density reduces typically as tree diameter increases (Ward et al., 2006). Thus, incorporation of drag effects into Manning coefficients approximates the first-order effect of mangroves on storm surges, which has been verified by significant improvement of surge simulation for Hurricane Wilma (Fig. 3). A similar treatment of bottom friction was employed to successfully simulate the effects of wetlands on storm surges along the coast of the Mississippi River Delta (Resio and Westerink, 2008; Loder et al., 2009; Wamsley et al., 2009, 2010). Therefore, the estimation of bottom friction coefficients in a storm surge model based on land cover is an effective way to simulate vegetation effects on storm surge flooding.

Storm surges as long waves are different from short-period wind waves. The decay of short-period waves across a mangrove zone occurs in a much faster rate than the decay of storm surges. Field measurements and theoretical analysis show that wind wave energy reduces by more than 50% within 40–80 m from the shore (Mazda et al., 1997; Möller et al., 1999). Therefore, even a narrow mangrove zone can significantly reduce the wind wave impacts, but this is not the case for storm surges. Kilometers of mangrove forests are needed to reduce surge heights to a less damaging level for a Category 3 hurricane like Wilma. For slowly moving Category 4 and 5 hurricanes, even a 15–30 km mangrove zone is not wide enough to completely attenuate storm surges. This has serious implications for developing vegetation greenbelts to protect people, infrastructure, and freshwater ecosystems in the coastal zone. The different requirements for widths of vegetation zones must be considered when bioshields are designed to defend the coast against impacts from wind waves and storm surges.

Storm surges and tsunamis are distinct from each other in several aspects. Storm surges are driven by wind stress and atmospheric pressure drops, and surge flooding can continue more than one day depending upon the forward speed of a hurricane. The maximum storm surge heights are seldom larger than 10 m along the Atlantic and Gulf Coasts of the United States. Storm surges have relatively low flow speeds over the land due to a slow inundation process. There is typically one surge peak during a hurricane event, although forerunners of storm surges exist in some cases as surge waves generated at the open ocean propagate to the shore. In contrast, a tsunami is often generated by propagation and transformation of waves generated by undersea earthquakes over the continent shelf and shallow nearshore zone. A tsunami travels at a faster speed of up to 800 km/h and with much shorter periods of 10–60 min (Alongi, 2008; Cochard et al., 2008). A tsunami can have a wave amplitude up to 30 m as it approaches the shore, as demonstrated by the case of the 2004 Indian Ocean tsunami (Alongi, 2008). Tsunami waves induce high velocity flows over the land that can damage mangrove trees. In addition, a train of waves including several peaks are often generated by the earthquake, which can reduce the protective function of mangroves by uprooting and removing trees several times during a tsunami. In spite of these differences, results from the current study on the mangrove effect on surge reduction can still provide useful insight on the protective role that the mangrove can play against tsunami waves because both surge and tsunami waves share the common characteristic of long waves. Since the attenuation of a mangrove forest is much more effective on surges from a rapidly moving (i.e., short-period) hurricane than from a slowly moving (i.e., long period) one, it is expected that a narrower mangrove zone can effectively attenuate a tsunami wave with the same amplitude as a surge wave and with a period shorter than the surge wave. Since large tsunamis have much higher amplitudes than storm surge waves, widths of mangrove zones required to reduce inundation

from large tsunami events are probably comparable to those for slowly moving, intense hurricanes, e.g., on the order of tens of kilometers. To derive a reliable estimation, the attenuation of mangroves on tsunami waves must be quantified using numerical models calibrated using rich field observations as demonstrated by this study.

## 7. Conclusions

The mangrove forests with widths of 6–30 km along the Gulf Coast of South Florida attenuated storm surges from Hurricane Wilma (Category 3) by reducing both the amplitude and extent of overland flooding, protecting the freshwater marsh behind the mangrove zone from surge inundation. Numerical simulations show that the inundation area by Wilma would extend more than 70% further inland without the mangrove zone, causing severe inundation of the wetlands behind the mangrove zone. The amplitude of storm surges at the front of the mangrove zone increase by 10–30% because of the “blockage” of mangroves to surge water, thus, structures in front of mangroves suffer more impacts than the case without mangroves. The decay rates of surge amplitudes are about 20–50 cm/km across mangroves, almost one order of magnitude higher than previous estimates. Without the mangrove zone, surge amplitudes would decrease gradually landward in almost a linear fashion with rates of 6–10 cm/km.

Numerical experiments indicate that widths of mangrove zones affect surge attenuation in a nonlinear fashion with large reduction at the initial increment of widths and small reduction at subsequent increments. A 7-to-8-km-wide mangrove zone which reduces amplitudes of Wilma's surges by about 80%, provides protection to the wetlands and structures behind the mangrove zone from surge impacts. Surges from a Category 5 hurricane with a rapid forward speed are also mostly restricted inside the mangrove zone, while surges from a Category 4 hurricane with a slow forward speed can penetrate through the mangrove zone. Storm surges from a slowly moving Category 5 hurricane, which reach 2–3 m high at the back of the mangrove zone, can still cause damage to the inland wetlands and structure. A mangrove forest with a width of tens of kilometers is needed to attenuate surge amplitudes from slowly moving, most intense hurricanes to a level which results in insignificant damage.

The numerical models such as CEST calibrated with field measurements provide a better estimation of the role of mangroves against surge inundation by appropriately separating the effect of vegetation from other correlated factors than statistical methods based on sparse samples. The incorporation of the drag force from mangrove trees into the bottom friction item by modifying Manning coefficients for various types of land cover is an effective way to simulate the effects of vegetation on surge inundation. The RMS error of computed peak surge heights within the mangrove zone for Hurricane Wilma is reduced from 0.9 m to 0.4 m by incorporating the effects of land cover, about 60% less than without incorporating land cover effects. High quality of coastal bathymetry and topography data such as those from LiDAR surveys is a prerequisite for producing reliable simulations of surge inundation.

## Acknowledgments

Drs. Keqi Zhang, Huiqing Liu, Yuepeng Li, and Hongzhou Xu were supported by a NOAA grant NA09NWS4680018. Dr. T.J. Smith III was supported by both the USGS Ecosystems Theme and Climate and Land Use Change Theme. He also received support from the Greater Everglades Priority Ecosystems Program. Any use of trade, product, or firm names is for descriptive purposes only and does not imply endorsement by the U.S. Government.

## References

- Alongi, D., 2008. Mangrove forests: resilience, protection from tsunamis, and responses to global climate change. *Estuarine, Coastal and Shelf Science* 76, 1–13.
- Baird, A., Bhalla, R., Kerr, A., Pelkey, N., Srinivas, V., 2009. Do mangroves provide an effective barrier to storm surges? *Proceedings of the National Academy of Sciences* 106, E111.
- Barbier, E., Koch, E., Silliman, B., Hacker, S., Wolanski, E., Primavera, J., Granek, E., Polasky, S., Aswani, S., Cramer, L., 2008. Coastal ecosystem-based management with nonlinear ecological functions and values. *Science* 319, 321.
- Blumberg, A., Kantha, L., 1983. Open boundary condition for circulation models. *Journal of Hydraulic Engineering* 112, 237–255.
- Bunya, S., Dietrich, J.C., Westerink, J.J., Ebersole, B.A., Smith, J.M., Atkinson, J.H., Jensen, R., Resio, D.T., Luettich, R.A., Dawson, C., Cardone, V.J., Cox, A.T., Powell, M.D., Westerink, H.J., Roberts, H.J., 2010. A high-resolution coupled riverine flow, tide, wind, wave, and storm surge model for Southern Louisiana and Mississippi. Part I. Model development and validation. *Monthly Weather Review* 138, 345–377.
- Castañeda-Moya, E., Twilley, R., Rivera-Monroy, V., Zhang, K., Davis, S., Ross, M., 2010. Sediment and nutrient deposition associated with Hurricane Wilma in mangroves of the Florida Coastal Everglades. *Estuaries and Coasts* 33, 45–58.
- Chatenoux, B., Peduzzi, P., 2007. Impacts from the 2004 Indian Ocean Tsunami: analysing the potential protecting role of environmental features. *Natural Hazards* 40, 289–304.
- Cochard, R., Ranamukhaarachchi, S., Shivakoti, G., Shipin, O., Edwards, P., Seeland, K., 2008. The 2004 tsunami in Aceh and Southern Thailand: a review on coastal ecosystems, wave hazards and vulnerability. *Perspectives in Plant Ecology, Evolution and Systematics* 10, 3–40.
- Dahdouh-Guebas, F., 2006. Coastal vegetation and the Asian tsunami. *Science* 311, 37.
- Danielsen, F., Sørensen, M., Olwig, M., Selvam, V., Parish, F., Burgess, N., Hiraishi, T., Karunakaran, V., Rasmussen, M., Hansen, L., 2005. The Asian tsunami: a protective role for coastal vegetation. *Science* 310, 643.
- Das, S., Vincent, J., 2009. Mangroves protected villages and reduced death toll during Indian super cyclone. *Proceedings of the National Academy of Sciences* 106, 7357.
- Desmond, G., 2003. Measuring and mapping the topography of the Florida Everglades for ecosystem restoration. In: Torres, A.E., Higer, L.A., Henkel, H.S., Mixson, P.R., Eggleston, J.R., Embry, T.L., Clement, G. (Eds.), *Greater Everglades Ecosystem Restoration Conference*, Palm Harbor, Florida.
- Feagin, R., 2008. Vegetation's role in coastal protection. *Science* 320, 176.
- Feagin, R., Mukherjee, N., Shanker, K., Baird, A., Cinner, J., Kerr, A., Koedam, N., Sridhar, A., Arthur, R., Jayatissa, L., 2010. Shelter from the storm? Use and misuse of coastal vegetation bioshields for managing natural disasters. *Conservation Letters* 3, 1–11.
- FEMA, URS Group Inc., 2006. Final Coastal High Water Mark Collection for Hurricane Wilma in Florida. Federal Emergency Management Agency, p. 103.
- Green, J., 2005. Modelling flow resistance in vegetated streams: review and development of new theory. *Hydrological Processes* 19, 1245–1259.
- He, R., Weisberg, R., 2002. Tides on the west Florida shelf. *Journal of Physical Oceanography* 32, 3455–3473.
- Hiraishi, T., Harada, K., 2003. Greenbelt Tsunami Prevention in South-Pacific Region. Port and Airport Research Institute, p. 23.
- Homer, C., Huang, C., Yang, L., Wylie, B., Coan, M., 2004. Development of a 2001 national land-cover database for the United States. *Photogrammetric Engineering and Remote Sensing* 70, 829–840.
- Houston, S.H., Shaffer, W.A., Powell, M.D., Chen, J., 1999. Comparisons of HRD and SLOSH surface wind fields in hurricanes: implications for storm surge and wave modeling. *Weather and Forecasting* 14, 671–686.
- Iverson, L., Prasad, A., 2007. Using landscape analysis to assess and model tsunami damage in Aceh province, Sumatra. *Landscape Ecology* 22, 323–331.
- Jelesnianski, C.P., Chen, J., Shaffer, W.A., 1992. SLOSH: Sea, Lake and Overland Surges from Hurricanes. NOAA, Washington, D.C., p. 71.
- Kathiresan, K., Rajendran, N., 2005. Coastal mangrove forests mitigated tsunami. *Estuarine, Coastal and Shelf Science* 65, 601–606.
- Kerr, A., Baird, A., 2007. Natural barriers to natural disasters. *Bioscience* 57, 102–103.
- Krauss, K., Doyle, T., Doyle, T., Swarzenski, C., From, A., Day, R., Conner, W., 2009. Water level observations in mangrove swamps during two hurricanes in Florida. *Wetlands* 29, 142–149.
- Large, W.G., Pond, S., 1981. Open ocean momentum flux measurements in moderate to strong winds. *Journal of Physical Oceanography* 11, 324–481.
- Loder, N.M., Irish, J.L., Cialone, M.A., Wamsley, T.V., 2009. Sensitivity of hurricane surge to morphological parameters of coastal wetlands. *Estuarine, Coastal and Shelf Science* 84, 625–636.
- Mattocks, C., Forbes, C., 2008. A real-time, event-triggered storm surge forecasting system for the state of North Carolina. *Ocean Modelling* 25, 95–119.
- Mazda, Y., Kobashi, D., Okada, S., 2005. Tidal-scale hydrodynamics within mangrove swamps. *Wetlands Ecology and Management* 13, 647–655.
- Mazda, Y., Magi, M., Kogo, M., Hong, P., 1997. Mangroves as a coastal protection from waves in the Tong King delta, Vietnam. *Mangroves and Salt Marshes* 1, 127–135.
- Möller, I., Spencer, T., French, J., Leggett, D., Dixon, M., 1999. Wave transformation over salt marshes: a field and numerical modelling study from North Norfolk, England. *Estuarine, Coastal and Shelf Science* 49, 411–426.
- National Ocean Service, 2005. Hurricane Wilma Preliminary Water Level Report. NOAA, Silver Spring, MD, p. 11.
- Nepf, H., 1999. Drag, turbulence, and diffusion in flow through emergent vegetation. *Water Resources Research* 35, 479–489.
- Olwig, M., Sørensen, M., Rasmussen, M., Danielsen, F., Selvam, V., Hansen, L., Nyborg, L., Vestergaard, K., Parish, F., Karunakaran, V., 2007. Using remote sensing to assess the protective role of coastal woody vegetation against tsunami waves. *International Journal of Remote Sensing* 28, 3153–3169.
- Petryk, S., Bosmajian, G., 1975. Analysis of flow through vegetation. *Journal of the Hydraulics Division of the American Society of Civil Engineers* 101, 871–884.
- Powell, M.D., Houston, S.H., Amat, L.R., Morisseau-Leroy, N., 1998. The HRD real-time hurricane wind analysis program. *Journal of Wind Engineering and Industrial Aerodynamics* 77&78, 53–64.
- Powell, M.D., Vickery, P.J., Reinhold, T.A., 2003. Reduced drag coefficient for high wind speeds in tropical cyclones. *Nature* 422, 279–283.
- Resio, D.T., Westerink, J.J., 2008. Modeling the physics of storm surges. *Physics Today* 61, 33–38.
- Simard, M., Zhang, K., Rivera-Monroy, V.H., Ross, M.S., Ruiz, P.L., Castañeda-Moya, E., Twilley, R.R., Rodriguez, E., 2006. Mapping height and biomass of mangrove forests in Everglades National Park with SRTM elevation data. *Photogrammetric Engineering and Remote Sensing* 72, 299–311.
- Smith III, T., Anderson, G., Balentine, K., Tiling, G., Ward, G., Whelan, K., 2009. Cumulative impacts of hurricanes on Florida mangrove ecosystems: sediment deposition, storm surges and vegetation. *Wetlands* 29, 24–34.
- Smith III, T., Robblee, M., Wanless, H., Doyle, T., 1994. Mangroves, hurricanes, and lightning strikes. *Bioscience* 44, 256–262.
- Soderqvist, L., Byrne, M., 2007. Monitoring the Storm Tide of Hurricane Wilma in Southwestern Florida, October 2005. U.S. Geological Survey, p. 16.
- Tanaka, N., 2009. Vegetation bioshields for tsunami mitigation: review of effectiveness, limitations, construction, and sustainable management. *Landscape and Ecological Engineering* 5, 71–79.
- Telis, P., 2006. The Everglades Depth Estimation Network (EDEN) for Support of Ecological and Biological Assessments. U. S. Geological Survey Fact Sheet 2006-3087, p. 4.
- Wamsley, T.V., Cialone, M.A., Smith, J.M., Atkinson, J.H., Rosati, J.D., 2010. The potential of wetlands in reducing storm surge. *Ocean Engineering* 37, 59–68.
- Wamsley, T.V., Cialone, M.A., Smith, J.M., Ebersole, B.A., Grzegorzewski, A.S., 2009. Influence of landscape restoration and degradation on storm surge and waves in southern Louisiana. *Natural Hazards* 51, 207–224.
- Ward, G., Smith III, T., Whelan, K., Doyle, T., 2006. Regional processes in mangrove ecosystems: spatial scaling relationships, biomass, and turnover rates following catastrophic disturbance. *Hydrobiologia* 569, 517–527.
- Xu, H., Zhang, K., Shen, J., Li, Y., 2010. Storm surge simulation along the U.S. East and Gulf Coasts using a multi-scale numerical model approach. *Ocean Dynamics* 60, 1597–1619.
- Yanagisawa, H., Koshimura, S., Goto, K., Miyagi, T., Imamura, F., Ruangrassamee, A., Tanavud, C., 2009. The reduction effects of mangrove forest on a tsunami based on field surveys at Pakarang Cape, Thailand and numerical analysis. *Estuarine, Coastal and Shelf Science* 81, 27–37.
- Zhang, K., 2011. Analysis of non-linear inundation from sea-level rise using LIDAR data: a case study for South Florida. *Climatic Change* 106, 537–565.
- Zhang, K., Simard, M., Ross, M., Rivera-Monroy, V.H., Houle, P., Ruiz, P., Twilley, R.R., Whelan, K.R.T., 2008a. Airborne laser scanning quantification of disturbances from hurricanes and lightning strikes to mangrove forests in Everglades National Park, USA. *Sensors* 8, 2262–2292.
- Zhang, K., Xiao, C., Shen, J., 2008b. Comparison of the CEST and SLOSH models for storm surge flooding. *Journal of Coastal Research* 24, 489–499.